HHS Public Access

Author manuscript

Transl Res. Author manuscript; available in PMC 2024 October 01.

Published in final edited form as:

Transl Res. 2023 October ; 260: 46–60. doi:10.1016/j.trsl.2023.05.007.

β-catenin/CBP activation of mTORC1 signaling promotes partial epithelial-mesenchymal states in head and neck cancer

Eric R. Reed[1,2,3], **Stacy A. Jankowski**[4,5], **Anthony J. Spinella**[6], **Vikki Noonan**[7], **Robert Haddad**[8], **Kenichi Nomoto**[9], **Junji Matsui**[9], **Manish V. Bais**[4], **Xaralabos Varelas**[6], **Maria A. Kukuruzinska**[4], **Stefano Monti**[2,3,10]

[1.]Data Intensive Studies Center, Tufts University, 177 College Ave., Medford, MA, 02155, USA

[2.]Section of Computational Biomedicine, Boston University School of Medicine, 75 E. Newton St., Boston, MA 02118, USA

[3.]Bioinformatics Program, Boston University, 24 Cummington St., Boston, MA 02115, USA

[4.]Department of Translational Dental Medicine, Boston University School of Dental Medicine, 635 Albany St., Boston, MA 02118, USA

[5.]Molecular and Translational Medicine Program, Boston University School of Medicine, 72 E Concord St., Boston, MA 02118, USA

[6.]Department of Biochemistry, Boston University School of Medicine, 72 E Concord St., Boston, MA 02118, USA

[7.]Division of Oral Pathology, Boston University School of Dental Medicine, 635 Albany St., Boston, Boston, MA 02118, USA

[8.]Department of Medical Oncology, Dana-Farber Cancer Institute, 450 Brookline Ave., Boston, MA 02215, USA

[9.]Eisai Inc., 200 Metro Blvd., Nutley, NJ 07110, USA

[10.]Department of Biostatistics, Boston University School of Public Health, 715 Albany St., Boston, MA 02118, USA

Abstract

Head and neck cancers, which include oral squamous cell carcinoma (OSCC) as a major subsite, exhibit cellular plasticity that includes features of an epithelial-mesenchymal transition (EMT),

Corresponding authors: Stefano Monti, Boston University School of Medicine, 75 E. Newton St. E611, Boston, MA, 02118, Phone: 617-358-7087, smonti@bu.edu, Maria A. Kukuruzinska, Boston University School of Medicine, 700 Albany St., W Building, Boston, MA 02118, Phone: 617-358-9690, mkukuruz@bu.edu, Xaralabos Varelas, Boston University School of Medicine, 71 E. Concord St., K620, Boston, MA 02118, Phone: 617-358-4575, xvarelas@bu.edu, Eric Reed, Data Intensive Studies Center, Tufts University, 177 College Ave., Medford, MA, 02155, USA, eric.reed@tufts.edu.

Data statement

The raw and processed microarray data of E7386 exposure of HSC3 cells have been deposited at GEO, accession number GSE190377. Analysis code can be accessed in Zenodo using the following URL, https://doi.org/10.5281/zenodo.6000515.

referred to as partial-EMT (p-EMT). To identify molecular mechanisms contributing to OSCC plasticity, we performed a multiphase analysis of single cell RNA sequencing (scRNAseq) data from human OSCC. This included a multi-resolution characterization of cancer cell subgroups to identify pathways and cell states that are heterogeneously represented, followed by casual inference analysis to elucidate activating and inhibitory relationships between these pathways and cell states. This approach revealed signaling networks associated with hierarchical cell state transitions, which notably included an association between β-catenin-driven CREB-binding protein (CBP) activity and mTORC1 signaling. This network was associated with subpopulations of cancer cells that were enriched for markers of the p-EMT state and poor patient survival. Functional analyses revealed that β-catenin/CBP induced mTORC1 activity in part through the transcriptional regulation of a raptor-interacting protein, chaperonin containing TCP1 subunit 5 (CCT5). Inhibition of β-catenin-CBP activity through the use of the orally active small molecule, E7386, reduced the expression of CCT5 and mTORC1 activity in vitro, and inhibited p-EMT-associated markers and tumor development in a murine model of OSCC. Our study highlights the use of multi-resolution network analyses of scRNAseq data to identify targetable signals for therapeutic benefit, thus defining an underappreciated association between β-catenin/CBP and mTORC1 signaling in head and neck cancer plasticity.

Introduction

Head and neck cancers comprise complex malignancies from multiple anatomical sites with distinct biology that collectively rank among the most deadly and disfiguring cancers [1–3]. Oral cavity cancer, which is a major subset (~40 – 50%) of head and neck cancers, presents primarily as smoking and alcohol associated oral squamous cell carcinoma (OSCC), and ranks among the most globally diagnosed cancers. Patients with OSCC frequently present with advanced disease characterized by locoregional spread to the cervical lymph nodes, which is predictive of distant metastases. Despite significant insights into genomic alterations in OSCC and advances in cytotoxic anticancer and taxane-based treatments, only two targeted therapies are available, an epidermal growth factor receptor-tyrosine kinase inhibitor (cetuximab) and immune checkpoint anti-programmed cell death-1-inhibitors (nivolumab and pembrolizumab), although they elicit limited responses in patients.

Mounting evidence indicates that evolution of OSCC to advanced disease entails a progressive acquisition of heterogeneous cell states endowed with new phenotypes in the absence of genetic mutations[4]. Such induction of new cell states, broadly defined as cell plasticity, involves epigenomic changes that promote chromatin accessibility with concomitant changes in gene expression signatures [5–7]. In carcinomas, epigenomic alterations of chromatin structure occur through the modification of histone tails that promote the development of high cellular plasticity states, such as partial epithelial-mesenchymal transition (p-EMT) and cancer stem cell (CSC)-like phenotypes [5,8]. Indeed, subpopulations of cells with a p-EMT phenotype, characterized by a spectrum of co-presenting epithelial and mesenchymal traits, have been identified at the invasive tumor front and shown to be associated with OSCC metastasis and poor disease prognosis in human patients [9–12].

CSC phenotypes and aggressive traits in OSCC and other cancer types have been associated with aberrant activation of the nuclear branch of the Wnt/β-catenin signaling pathway through the interaction of β-catenin with the histone acetyltransferase cAMP-responsive element binding (CREB)-binding protein (CBP)[7,13–22]. Small molecule inhibitors of the β-catenin-CBP interaction, such as ICG-001 [7] and E7386[23,24], block oncogenic traits in cellular and murine models of OSCC and other carcinomas [7,24].

To gain insights into the molecular mechanisms underlying cell plasticity and the induction of p-EMT phenotypes in OSCC, we applied newly developed computational tools to the analysis of single-cell RNA sequencing (scRNAseq) data from oral cavity squamous cell carcinomas. Our driving hypothesis was that a systems-level analysis of the molecular heterogeneity in OSCC would help us elucidate the contribution of β-catenin/CBP signaling to oral tumorigenesis. Multi-resolution characterization of these data identified cell subtypes with a range of β-catenin/CBP activity, and showed that high β-catenin/CBP activity was associated with p-EMT cellular states[10] and predictive of low patient survival. Significantly, our analyses predicted that β-catenin/CBP signaling promotes the p-EMT state in OSCC through activation of the mTOR Complex 1 (mTORC1) signaling pathway. In silico functional analysis further predicted that β-catenin/CBP activates mTORC1 via transcriptional regulation of genes encoding regulators of raptor, including chaperonin containing TCP1 subunit 5 (CCT5), which has been shown to recruit raptor into the T-complex protein Ring Complex (TRiC) required for mTORC1 complex formation [25]. Molecular experiments in OSCC cell lines demonstrated that β-catenin/CBP promotes CCT5 protein expression and mTORC1 signaling and that these signals are crucial for the p-EMT state. Further, small molecule inhibition of β-catenin/CBP activity reduced the levels of markers associated with mTORC1 activation and the p-EMT state and halted the development of tumors in the 4-Nitroquinoline 1-oxide (4NQO) carcinogen-induced model of OSCC [26]. Collectively, our analyses highlight the importance of β-catenin/CBP pathway activity in OSCC progression and demonstrate its key role in the induction of mTORC1 signaling and activation of the p-EMT state that contributes to poor survival in human patients [10].

Materials and Methods

Statistical analysis

Analyses of high-throughput transcriptomic and protein expression data were performed in R (v4.1.0). Multiple hypothesis corrections of p-values of these analyses were performed using Benjamini-Hochberg false discovery rate (FDR) correction [27]. Analyses of immunoblots, reverse transcription quantitative polymerase chain reaction (RT-qPCR), and immunofluorescence experiments were performed in GraphPad Prism (v9) using an unpaired Student’s t-test. All reported p-values are two-sided.

Experimental models

Experiments modeling changes in β-catenin/CBP activity were performed via pharmacological inhibition of β-catenin-CBP interaction with E7386 (Eisai Co., Ltd.), diluted in 0.1% dimethyl sulfoxide (DMSO) (Sigma).

Cell model experiments were performed using male OSCC patient cell lines, HSC3 (XenoTech) and CAL27 (XenoTech). All Cells were cultured at 37°C under 5% CO_2 in Dulbecco's modified Eagle's medium (DMEM) (Life Technologies) supplemented with 10% heat inactivated fetal bovine serum (FBS) (Life Technologies) and 1% penicillin/streptomycin (Life Technologies).

Mouse model experiments were performed with C57BL/6 mice (Jackson Laboratories).. These mice were housed under standard conditions in the animal facility of Boston University School of Medicine. All procedures were performed based on Boston University's Institutional Animal Care & Use Committee (IACUC).

Transcriptomic signature of β-catenin/CBP activity in HSC3 cells

In a previous study we identified a transcriptional signature of β-catenin/CBP activity based on microarray profiling of ICG-001 treatment response in HSC3 cells[7]. In this study, using a similar experimental design, we identified a transcriptional signature of β-catenin/CBP activity by microarray profiling of E7386 treatment response in HSC3 cells. Three separate wells (triplicate) in 6-well plates were seeded with HSC3 cells (at 5×10^4/well). After 12–24 h (i.e., ~ 50% confluency), the cells were treated with either 0.1% dimethyl sulfoxide (DMSO) or 0.1 μM E7386 in DMSO. After 48–64 h, the cells were trypsinized and harvested for RNA purification using the miRNeasy Micro Kit (QIAGEN no. 217084). Gene expression profiling was performed in triplicates per treatment group (n = 3) using Affymetrix Human Gene 2.0ST arrays. We have been deposited these data on the Gene Expression Omnibus (GEO), accession number GSE190377.

Raw expression values of HSC3 cells were normalized together using the Robust Multiarray Average (RMA) with the affy R package (v1.41.1)[28]. A BrainArray Chip Definition File (CDF) was used to map the probes on the array to unique Entrez Gene identifiers (http://brainarray.mbni.med.umich.edu/Brainarray/Database/CustomCDF). Differential gene expression analysis with respect to E7386 treatment was performed using the limma R package (v3.14.4)[29]. Genes that were not expressed above the array-wise median value of at least one array were removed from the analysis. Only genes with absolute linear fold-change ≥ 1.5 and filtered FDR q ≤ 0.01 were considered and used for further analysis as the E7386 treatment gene set.

Single-cell transcriptomics data processing

Published scRNAseq profiles from human oral cavity HNSCC patient tissues originally generated by *Puram et al.*[10] were obtained from GEO, accession number GSE103322. The original data included transcripts-per-million counts (TPM) of 23,686 genes, and 5,902 cell profiles across 18 HNSCC patient samples. Of the 5,902 cell profiles, 2,215 were previously labelled as cancer cells, with 1,427 and 788 originating from HNSCC and lymph node, respectively[10]. Furthermore, the cell profiles were generated using two separate reverse transcriptase (RT) methods, with 1,587 and 628 of the 2,215 cancer cell profiles prepared using Superscript 2 and Maximum RT methods, respectively[10].

Integration of cancer cell profiles originating from different patients and RT technologies and subsequent clustering analysis were performed using the Seurat R package (v3.0.0)[30].

Prior to data integration, cell profiles with fewer than 200 genes with counts > 0 were removed. Next, the groups of cell profiles selected for integration were defined based on a combination of patient-of-origin and RT methods used in the library preparation. Integration groups with fewer than 100 cell profiles were removed. After filtering, the final data included 1,760 cells across seven patients, with 1,071 and 689 profiles originating from HNSCC and lymph node, respectively, and 1,251 and 509 profiles generated with Superscript 2 and Maxima RT methods, respectively. Following log-normalization of TPM gene expression values, integration of the seven samples was performed in three steps. First, the top 2,000 most variable features were identified for each sample, independently using the *FindVariableFeatures( )* function. Subsequently, anchoring features between data were identified using *FindIntegrationAnchors()* function, with the k.filter argument set to 100. Finally, data from the seven samples were integrated using the *IntegrateData()* function. Clustering was performed on the first 25 principal components using the *RunPCA()*, *FindNeighbors()*, and *FindClusters()* functions. For visualization, Uniform Manifold Approximation and Projection (UMAP) was performed using the *RunUMap()* function. For downstream analysis, the integrated data were corrected to remove extraneous signal originating from cells in G2M and S phase cell cycle using the *CellCycleScoring()* and *ScaleData()* functions. Chi-squared contingency table tests were performed to assess the composition of each cluster versus cell type (e.g., HNSCC, lymph node), RT method, and patient.

Single-cell cluster subgrouping and annotation

K2Taxonomer (K2T) nested subgrouping and annotation of Seurat clusters was performed using the K2Taxonomer R package (v1.0.5)[31]. Recursive partitioning of the cell profile clusters was performed with 500 bootstrap samples per partition and constrained k-means[32], yielding a set of nested subgroups, each subgroup corresponding to a node in the K2T dendrogram. Gene-level and pathway-level differential analyses using limma[29] were performed between every two subgroups children of a common parent (sub)group, yielding subgroup-specific signatures. For pathway-level differential analyses, each cell profile was first projected on a curated list of gene sets using Gene Set Variation Analysis (GSVA) (v1.40.1)[33]. These annotation gene sets included: six 100-transcript gene sets reported by *Puram et al*[10], which define cell states in HNSCC scRNAseq profiles (Cell Cycle, p-EMT, Epithelial Differentiation 1, Epithelial Differentiation 2, Stress, Hypoxia); the 50 hallmarks of human cancer pathways from the Molecular Signatures Database (mSigDB) (v7.0)[34,35]; two miRNA target gene sets from TargetScan (v7.2)[36] (*miR-143*, *miR-145*); and two separate sets of genes up- and down-regulated by β-catenin/CBP signaling following pharmacological inhibition of β-catenin/CBP activity in HSC3 cell lines with ICG-001 and E7386, respectively. The ICG-001 gene sets were reported in[7], while the E7386 gene sets were generated as described above. Importantly, given that each of the β-catenin/CBP gene sets represent inhibition of that pathway, the interpretation of the gene sets was reversed, such that, throughout this manuscript, genes that were down-regulated by inhibition of β-catenin/CBP are referred to as genes up-regulated by β-catenin/CBP activity, and vice versa.

Enrichment scores of complementary up- and down-regulation of signal pathways were aggregated using the *aggregateGSVAscores()* K2Taxonomer function. This function computes the score difference of the enrichment scores calculated from the two sets of genes up- and down-regulated by a given pathway, respectively. These gene sets included: Hallmark UV Response, Hallmark KRAS signaling, β-catenin/CBP (E7386), and β-catenin/CBP (ICG-001).

Survival analysis of single-cell cluster subgroup signatures on HNSCC data

Survival analysis was conducted by scoring The Cancer Genome Atlas (TCGA) HNSCC bulk RNAseq profiles[37], obtained from the Genomic Data Commons (GDC) (https://portal.gdc.cancer.gov), according to their GSVA-based projection onto the top genes from each K2T subgroup signature. These publicly available data included 36,812 individual genes from 499 primary tumor samples of individual patients. Among the 499 individual patients, measured 5-year survival included 301 survivors and 197 deceased patients. Mean, standard deviation, minimum, and maximum age at diagnosis was 61.56, 11.91 19.99, and 90.00 years, respectively. Counts were normalized to log counts-per-million following trimmed-mean of M values scaling using the edgeR R package (v3.34.0)[38].

For the survival analysis of the 499 TCGA HNSCC tumor bulk expression profiles, signatures were first defined for each K2T-derived scRNAseq subgroup as the top 50 genes based on p-value ranking (low-to-high) of differential expression comparing sibling subgroups at each partition. TCGA HNSCC data were then projected onto each of these signatures using GSVA. Association between each GSVA-based signature score and 5-year survival rate was carried out using multivariate Cox proportional hazards modeling, controlling for age at diagnosis.

Interaction between pathways and cell states

Causal inference analysis was performed on the scRNAseq GSVA-based enrichment scores from the top pathways and cell states identified as highly differentially regulated between K2T estimated subgroups. Cell profiles characterized primarily by high cell cycle activity were excluded from this analysis due to overrepresentation in these data. Causal inference was performed using the Peter and Clark algorithm[39] as implemented in the *pcalg* R package (v2.7–3)[40]. Briefly, the algorithm builds a sparse, partially directed graph where the nodes represent the input variables (here, the top pathways represented by their GSVA scores), and the absence of an edge between two variables represent the absence of an unmediated dependence between those variables. The algorithm first identifies all the pairwise unmediated dependencies (undirected edges) between the input variables based on conditional independence tests. It then establishes the directionality of the edges, when possible, based on the concept of a collider test[41], whereby a variable triplet's undirected graph, X – Z – Y, yields the directed graph, X→Z←Y, if specific conditions of conditional (in)dependence are satisfied, namely, if X and Y are marginally independent, but become dependent when conditioned on Z. Since the software does not report estimates of the "strength" of the inferred pairwise causal relationships, partial correlation testing was used among the causally related variables to estimate the strength and sign (i.e., positive or negative) of their association.

Identification of transcriptional mediators between β-catenin/CBP and mTORC1 signaling

Functional analyses to identify the potential causal mediators between β-catenin/CBP and mTORC1 pathway activities in the scRNAseq data were carried out using a strategy based on the Spearman correlation between the expression of each of the 19,862 individual genes and enrichment scores of each pathway corresponding to β-catenin/CBP (E7386 and ICG-001) and mTORC1. As with causal inference analyses, cell profiles characterized primarily by high cell cycle activity were excluded. Gene-specific candidacy for potential causal relationships was evaluated by ranking the genes based on the minimum of the Spearman correlations of each gene (high-to-low) with the three pathway variables.

Next, these rankings were tested for enrichment with pathways of interest using pre-ranked gene set enrichment analyses (GSEA)[34] with 2000 permutations. These gene sets included p-EMT-specific genes[10] and genes encoding raptor-interacting proteins[42], as well as the β-catenin/CBP and mTORC1 gene sets. Since each of the two gene sets of β-catenin/CBP signaling (E7386 and ICG-001), included up- and down-regulated gene sets, each of these four total gene sets were tested separately.

The scRNAseq-based findings were replicated in two independent datasets, which included the TCGA HNSCC bulk RNAseq data and transcriptomics and proteomics profiles from upper aerodigestive track cell lines in the Cancer Cell Line Encyclopedia (CCLE)[43] (https://portals.broadinstitute.org/ccle).

For the replication based on TCGA HNSCC data, we performed analyses across all 499 TCGA HNSCC tumor profiles as well as within six stratifications of the patients based on HPV status, HPV- and HPV+, and on four previously reported molecular subtypes in HPV- samples, classical, basal, mesenchymal, and atypical[37]. Subtype labels were obtained from the GDC using the TCGAbiolinks R package (v 2.22.4)[44–46]. According to available labeling, these analyses comprised: 408 HPV-, 89 HPV+, 44 HPV- classical, 75 HPV- basal, 65 HPV- mesenchymal, and 35 HPV- atypical tumor profiles. To account for the potential confounding effect of tumor purity, association between gene expression and each of the three pathway variables of interest were estimated using Spearman *partial* correlation, conditioning on covariates accounting for stromal and immune infiltration scores. These scores had been previously measured on the TCGA data using the Estimation of STromal and Immune cells in MAlignant Tumours using Expression data (ESTIMATE) method, and were obtained from The University of Texas MD Anderson Cancer Center ESTIMATE database (https://bioinformatics.mdanderson.org/estimate/)[47].

For the replication based on CCLE data, we performed analyses based on normalized counts for 17,629 total genes shared with the HNSCC scRNAseq data across single samples from 32 untreated cell lines. Additionally, we used Spearman correlation to examine the relationships between gene-expression and reverse-phase protein array (RPPA)-based expression of three of 214 measured proteins: mTOR, raptor, and phosphorylated β-catenin (pT41/S45)[48]. This analysis was performed using single samples from 30 untreated cell lines shared between the gene and protein expression data.

Cell line immunoblot validation experiments

Biochemical validation of the β-catenin/CBP and mTORC1 interaction was performed by immunoblot analysis of HSC3 and CAL27 OSCC cell lines. Prior to treatment, cells were seeded in 10 cm dishes and cultured to reach 70%–80% confluency at the end of 48 hours or 50%–60% confluency at the end of 24 hours. About 12 hours after seeding, cells were treated with vehicle (0.1% DMSO), and 1 μM E7386 or 0.1 μM E7386. Cells were washed in PBS, lysed and collected in Triton-X-100/β-octylglucoside buffer containing protease and phosphatase inhibitors (Halt, ThermoScientific). Extracted proteins were quantified using a Pierce BCA Protein Assay Kit (ThermoFisher). Total cell lysates (15–20 μg) were fractionated on 4–20% Mini-PROTEAN TGX Precast gels (BioRad), and proteins were transferred onto a PVDF membrane via wet transfer. Membranes were incubated for 1 hour at room temperature in a blocking solution of 5% milk in TRIS Buffered Saline/0.1% Tween (TBS-T) or 5% BSA in TRIS Buffered Saline containing 0.1% Tween (TBS-T) for phosphorylated proteins. Membranes were incubated overnight at 4°C with primary antibodies and followed by incubation with HRP-linked secondary antibodies for 1 hour at room temperature. Primary antibodies used were: phosphorylated S6K (p-S6K) (Thr389) (Cell Signaling Technologies, cat#9234), S6K (Cell Signaling Technologies, cat#2708), raptor (Cell Signaling Technologies, cat#2280), CCT5 (Abcam, cat#ab129016), and GAPDH (Cell Signaling Technologies, cat#5174). Immunostained proteins were visualized using SuperSignal West Pico PLUS Chemiluminescent Substrate (ThermoFisher) and images were acquired using Bio-Rad ChemiDoc MP Imaging System. To detect both p-S6K and S6K total abundance, membranes were stripped using Restore PLUS Immunoblot Stripping Buffer (ThermoScientific), tested for stripping efficacy, blocked again for 30 minutes at room temperature, and then incubated overnight at 4°C with primary antibodies.

Immunoblots were quantified using ImageJ[49]. Expression levels of target proteins were normalized to GAPDH and then fold change was calculated with respect to cells treated with DMSO. Three independent biological replicates were used for each experimental condition. Analyses comparing differences in mean expression levels between treatment groups were performed using GraphPad Prism (GraphPad Software Inc.) using an unpaired Student's t-test. Statistical significance was determined using a p-value threshold of 0.05.

Targeted gene expression in-vitro experiments

RT-qPCR-based evaluation of changes in expression of *CCT5* and selected p-EMT marker genes was performed on HSC3 cells following pharmacological inhibition of β-catenin/CBP with E7386 and small interfering RNA (siRNA)-based knockdown of *CCT5*. Non-Target siRNA (Dharmacon) were transfected into HSC3 cells with Lipofectamine RNAiMAX (Invitrogen, 56532) and incubated for 48 hours. Cell lysates were then collected, and RNA was purified with the RNeasy Mini Prep Kit (Qiagen, 74106) per manufacturer's instructions. E7386 (Eisai Co., Ltd.) or DMSO (Fisher Chemical, D128500) were administered at a 1 μM concentration to HSC3 cells and incubated for 24 hours. Cells were then washed and incubated in DMEM (Gibco, 11995065) for an additional 24 hours. Total RNA was then collected and purified with the Rneasy Mini Prep Kit (Qiagen, 74106) per manufacturer's instructions. RNA from experimental HSC3 cells was extracted with the Rneasy Mini Prep Kit (Qiagen, 74106) per manufacturer's instructions then cDNA

libraries were prepared with the iScript cDNA Synthesis Kit (BioRad, 1708891). RT-qPCR gene expression analyses were carried out on the ViiA 7 Real-Time PCR System (Applied Biosystems) using TaqMan Universal Master Mix II, with UNG (Applied Biosystems, 4440038) and TaqMan probes (Life Technologies). TaqMan probes used in this study are listed in Supplemental Table S1.

Target gene transcript levels were quantified using the ΔΔCt method and normalized to GAPDH. Independent biological replicates (n = 4–6) were used for each experimental condition. Analyses comparing differences in mean expression levels between treatment groups were performed using GraphPad Prism (GraphPad Software Inc.) using an unpaired Student's t-test. Statistical significance was determined using a p-value threshold of 0.05.

Mouse model hematoxylin and eosin (H&E) and immunofluorescence experiments

For induction of OSCC, seven-week-old mice were treated with drinking water containing 50 μg/ml 4-nitroquinoline 1-oxide (4NQO) for 16 weeks and then given with normal drinking water for another 8–10 weeks. E7386 was given at 50 mg/kg (body weight) by oral gavage daily, starting at week 19 until week 22. Mice were sacrificed on week 23, tongues were dissected and processed for hematoxylin and eosin (H&E) and immunofluorescence analyses as described below.

H&E analysis was performed by iHisto Histopathology Support. In brief, formalin-fixed sections were deparaffinized before being stained with eosin for cytoplasmic visualization and Hematoxylin for nuclei. Staining and imaging was performed with Leica ST5020 Autostainer w/CV5030 Slide Coverslipper & TS5025 Transfer Station.

Formalin-fixed sections were deparaffinized in graded xylene and ethanol and rinsed in deionized water. For antigen retrieval, slides were placed in Antigen Unmasking Solution (Vector Laboratories) in a pressure cooker at high pressure for 15 minutes. Samples were brought to room temperature by rinsing with deionized water and blocked in 5% FBS in PBS and Rodent Block M (Biocare Medical). After washing in PBS, samples were incubated with primary antibodies overnight at 4°C. The next day, samples were washed with PBS and incubated with secondary antibodies for 1 hour at room temperature in the dark. Sections were washed with PBS before incubation with DAPI for 10 minutes at room temperature in the dark. Coverslips were applied with Prolong Diamond Antifade Mountant (Invitrogen). Fluorescence intensity was measured using ImageJ software (v.2.3.0). Slides were imaged with Zeiss LSM 710-Live Duo Confocal with 2-Photon Capability using Zen software (v3.5) to capture tumor and dysplasia areas. Relative fluorescence intensity for each channel was measured using ImageJ software. Three and two biological replicates of tongue samples were used for 4NQO and 4NQO + E7386 treated mice, respectively. Quantification of podoplanin was performed on multiple non-overlapping 200um-by-200um images per sample, from which relative fluorescence intensity was measured from multiple non-overlapping areas of either dysplasia or squamous cell carcinoma, resulting in between 3–12 images per sample, and 6–11 areas per image. Testing of differences between mean log(relative immunofluorescence intensity) of podoplanin of 4NQO + E7386 to 4NQO treatment was performed with a linear mixed model comprising treatment group as a fixed

effect to be tested and image identifier as a random effect using the lmerTest R package (v3.1–3)[50].

Results

Multi-resolution characterization of scRNAseq cell profiles defines a taxonomy of diverse cellular states in OSCC.

To elucidate signaling networks and cell states that contribute to OSCC heterogeneity we identified and functionally annotated data-driven subgroups of 1,760 scRNAseq profiles of primary tumor and lymph node tissue from seven oral cavity HNSCC patients[10]. To this end, we employed the K2T recursive partitioning workflow[31] to estimate nested relationships between 14 cell clusters estimated by Seurat. K2T uses a recursive partitioning algorithm to identify and annotate a nested taxonomy (i.e., grouping) of cell types defined by distinct transcriptional programs, thereby facilitating biological investigation at multiple levels of resolution.

The taxonomic subgroups defined by K2T were annotated based on their enrichment-based differential association with a curated set of cell states and signaling pathways. The taxonomy and annotated subgroups are summarized in Fig. 1A–C and Table 1. The first major partition separated profiles into mTORC1 expressing (A2) and non-expressing cell types, followed by sub-partitions driven by the up-regulation (C2) or down-regulation (B2) of β-catenin/CBP, and up-regulation (F1) of p-EMT, among others. The complete results from partition-level differential gene and pathway analyses are shown in Supplemental Tables S2 and S3, respectively.

Cells within the C2 subgroup were also enriched in genes encoding cell cycle regulators, and the subgroups E1 and J1 were associated with epithelial differentiation. The epithelial differentiation cell state was here captured in two distinct gene sets reported as likely representing different degrees of differentiation[10], and labelled epithelial differentiation 1 – defined by up-regulated EPCAM and Krt16, among others, and epithelial differentiation 2 – defined by up-regulated KRT17/25 and KLK5/11, among others. Finally, subgroup F1 was associated with p-EMT. Signaling pathways associated with different taxonomic subgroups included mTORC1, (A2, C2, B2, and J2), β-catenin/CBP (C2, B2, and E1), Myc (C2, E1, and J2), and TNFα/NFκB (F1), and *miR-145* (J2).

Results of the survival analysis of TCGA HNSCC patients stratified according to their GSVA-based projection[33] onto K2T-derived signatures are shown in Fig. 1A and Table 2. Better patient survival (Hazard Ratio < 1, FDR < 0.1) was found for projections onto subgroup signatures with lower enrichment of β-catenin/CBP and/or mTORC1 signaling, as well as higher enrichment of epithelial differentiation (subgroups B2, E1, and J2). Conversely, worse patient survival (Hazard Ratio > 1, FDR < 0.1) was found for subgroup signatures associated with higher enrichment of TNFα/NF-κB signaling and p-EMT (subgroup F1). Kaplan-Meier curves illustrating survival of TCGA HNSCC patients, stratified by projections onto signatures from these four subgroups are shown in Fig. 1D.

In summary, taxonomy discovery followed by differential enrichment analysis among the estimated taxonomic groups in the scRNAseq data (Fig. 1B,C), and survival analysis based on projection of TCGA bulk profiles onto the single cell-derived signatures (Fig. 1D), identified five pathways (mTORC1, Wnt/β-cat/CBP, Myc, TNFa/NF-kb, and miR145) and three cell states (cell cycle, epithelial differentiation, and pEMT) whose complex relationships were the focus of downstream analysis.

Causal inference analysis indicates that β-catenin/CBP signaling activates mTORC1 signaling in the p-EMT state observed in OSCC.

To delineate direct and indirect relationships between signaling pathways (mTORC1, β-catenin/CBP, Myc, TNFα/NF-κB, and *miR-145*) enriched in distinct cell state subgroups (cell cycle, epithelial differentiation, and p-EMT) we performed causal inference analysis[39] on the GSVA enrichment scores of these pathways. Two separate models were estimated, based on separate β-catenin/CBP-regulated gene sets corresponding to pharmacological inhibition of β-catenin/CBP activity using E7386[23,24] and ICG-001[7] (Fig. 2A, Supplemental Table S4). Due to its role in OSCC progression, we had a particular interest in defining causal relationships implicated in the induction of the p-EMT state.

In both models, mTORC1 demonstrated the strongest direct induction of p-EMT, with partial correlation estimates of 0.37 (FDR = 1.25E-43) and 0.36 (FDR = 2.06E-41) in the E7386 and ICG-001 models, respectively. TNFα/NFκB also demonstrated direct induction of p-EMT across both models, but had markedly lower association, with partial correlation estimates of 0.22 (FDR = 1.01E-14) and 0.22 (FDR = 3.66E-15), respectively.

The strongest inferred direct pathway-to-pathway interaction was the activation of mTORC1 by β-catenin/CBP based on the E7386 β-catenin/CBP inhibition gene signature model, with a partial correlation of 0.36 (FDR = 2.61E-40). A similar association between mTORC1 and β-catenin/CBP was inferred in the ICG-001 β-catenin/CBP inhibition gene signature model, although this causal relationship showed an indirect activation of mTORC1 by β-catenin/CBP that was mediated by activation of Myc, with partial correlation estimates of β-catenin/CBP to Myc and Myc to mTORC1 of 0.23 (FDR = 1.77E-16) and 0.27 (FDR = 1.40E-22), respectively. Both models also inferred inhibition of mTORC1 by *miR-145*, with partial correlation estimates in the E7386 and ICG-001 models of −0.25 (FDR = 5.84E-20) and −0.19 (FDR = 3.87E-12), respectively.

Taken together, these causal models predicted induction of p-EMT by mTORC1, with upstream activation by β-catenin/CBP and Myc signaling, along with inhibition by *miR-145*.

Functional analysis suggests that β-catenin/CBP activates mTORC1 via transcriptional regulation of genes encoding raptor-interacting proteins

Due to the previously described importance of β-catenin/CBP and mTORC1 in OSCC[7,13,14,16,17,21,51,52] we chose to follow-up on the newly identified relationship between these pathways and p-EMT. To this end, to prioritize potential mediators of β-catenin/CBP and mTORC1, we initially performed a correlation-based assessment of the association between the two pathways of interest and each of the genes in the transcriptome. For each gene, this shared association was defined as the minimum Spearman correlation between

its expression and each of three enrichment scores corresponding to the mTORC1 gene set and the two β-catenin/CBP gene sets (E7386 and ICG-001). This analysis was first performed on the scRNAseq data and then replicated in TCGA HNSC bulk gene expression and CCLE gene expression and proteomics data from upper airway cancer cell lines[43] (Fig. 3A–D, Supplemental Table S5). To assess the generalizability of functional results across molecularly defined HNSCC categories, TCGA HNSCC analyses were carried out across all tumor samples, as well as within six different stratifications based on HPV status, and on four previously reported HPV- molecular subtypes, classical, basal, mesenchymal, and atypical[37] (Fig. 3B, Supplemental Fig. S3, Supplemental Table S6).

Analysis of the scRNAseq data revealed that all eight subunits of the TRiC complex, a multi-protein chaperonin complex that plays a direct role in folding mTORC1-components, raptor and mLST8[25], were highly associated with mTORC1 and β-catenin/CBP signaling. These TRiC subunits were within the top 2.5 percentile of genes most highly associated with mTORC1 and β-catenin/CBP signaling (Fig. 3A), and *CCT5*, which encodes one of the subunits, was the most highly associated with mTORC1 and β-catenin/CBP signaling (min. correlation = 0.407, FDR = 2.15E-50). These findings were independently replicated in the TCGA HNSCC bulk gene expression data and in the CCLE upper aerodigestive track cancer cell line data. In the TCGA HNSCC tumor samples, all eight TRiC genes were within the top 4.4 percentile of genes most highly associated with mTORC1 and β-catenin/CBP signaling (Fig. 3B, Supplemental Table S5). Moreover, across the six tumor subtypes analyzed, the maximum percentile of these genes ranged from 3.3 to 30.0, in HPV- and HPV- classical, respectively (Supplemental Fig. S1, Supplementary Table S5). Finally, in the CCLE data all TRiC genes were within the top 8.4 percentile (Fig. 3C, Supplementary Table S5).

To investigate whether additional genes encoding factors that bind with mTORC1 components could potentially mediate activation of mTORC1 by β-catenin/CBP signaling, a published set of genes coding for raptor-binding proteins[42] was tested against the minimum Spearman correlation-based gene scores by rank-based GSEA[34]. The statistical results of these analyses are shown in Table 3 and Supplemental Table S6, and the position of each gene in the rankings is shown in Fig. 3A–C and Supplemental Fig. S1. In all analyses of the scRNAseq, TCGA HNSCC, and CCLE data, genes encoding raptor-binding proteins were positively associated with the minimum correlation-based ranking (FDR= 1.00E-3, 4.90E-2, 1.17E-3, respectively). For TCGA HNSCC, all stratified analyses were statistically significant with FDR= 4.90E-2, which was the smallest value achieved after multiple hypothesis correction. Moreover, for genes encoding raptor-binding proteins in CCLE data, there was an observed general congruence between gene-level correlation with each of the three pathways' enrichment scores and protein levels of mTORC1, raptor, and phosphorylated β-catenin (pT41/S45) (Fig. 3D). Negative Spearman correlation of these genes with the levels of phosphorylated β-catenin (pT41/S45) was indicative of a greater abundance of functional β-catenin, as pT41/S45 is associated with β-catenin degradation[53].

Importantly, p-EMT genes were significantly positively associated with correlation-based rankings of genes in both the scRNAseq and the full TCGA HNSCC data (FDR = 1.00E-3 and 4.90E-2, respectively). The same trend and significance level were observed in all

TCGA HNSC subtypes except for HPV- Atypical (FDR = 0.57). We did not observe the same trend in the CCLE data (FDR = 0.12), which is likely due to underrepresentation of cells undergoing p-EMT in these data.

Taken together, these findings suggest that β-catenin/CBP signaling induces genes that code for regulatory proteins of the mTORC1 complex, such as the TRiC genes of which *CCT5* is the most tightly regulated, subsequently resulting in the activation of mTORC. Moreover, they support the notion that this cascade is involved in the induction of p-EMT across multiple HNSCC subtypes.

Biochemical analyses confirm that mTORC1 and CCT5 function downstream of the β–catenin/CBP axis.

To validate that mTORC1 activity and CCT5 expression are regulated downstream of β-catenin/CBP in head and neck cancer cells, we performed immunoblot experiments with two human OSCC cell lines, CAL27 and HSC3, following pharmacological inhibition of β-catenin/CBP with E7386. Specifically, the phosphorylation status of mTORC1 target protein, S6K, at Thr389, as well as the abundance of CCT5 and raptor proteins were assessed, where the latter is functionally dependent on CCT5 as a component of the mTORC1 complex. The immunoblots representing these data are shown in Supplemental Fig. S1. The levels of phosphorylated S6K (p-S6K) relative to total S6K and the abundance of CCT5 were significantly reduced in both cell lines in response to E7386 treatment at concentrations of 0.1 μM and 1 μM, relative to the vehicle treated cells (p-S6K/S6K max. p-value = 0.0019, CCT5 max. p-value = 0.02) (Fig. 4A, B, Supplemental Table S7). The levels of total S6K were less affected by E7386 treatment, with the only significant change in total S6K observed in CAL27 cells treated with 1 μM E7386 (p-value = 0.0284) (Fig. 4A, Supplemental Table S7). Furthermore, we did not observe changes in raptor (Fig. 4B, Supplemental Table S7).

These findings demonstrate that both mTORC1 activity and CCT5 expression are reduced following inhibition of β-catenin/CBP, thus confirming our in-silico predictions that mTORC1 activity and CCT5 expression are regulated downstream of β-catenin/CBP.

CCT5 is required for the expression of p-EMT genes downstream of β-catenin/CBP in OSCC cells

To assess whether transcriptional regulation of *CCT5* by β-catenin/CBP mediated the activation of p-EMT, we evaluated the consequences of *CCT5* siRNA-mediated depletion on selected p-EMT gene expression, compared with pharmacological inhibition of β-catenin/CBP with E7386. The five p-EMT genes selected were a subset of p-EMT genes previously identified[10], which were positively correlated with GSVA-based projections of both β-catenin/CBP and mTORC1 gene sets and differentially regulated across multiple K2T derived subgroups (Supplemental Fig. S3). Knockdown of *CCT5* resulted in a significantly reduced expression of several p-EMT-associated genes, including podoplanin (*PDPN*), alpha-actinin-1 (*ACTN1*) and galectin 1 (*LGALS1*), mirroring observations following inhibition of β-catenin/CBP with E7386 (Fig. 4C, Supplemental Table S8). The changes in *CCT5* expression following inhibition of β-catenin/CBP with E7386 agreed with

immunoblot analyses, supporting the transcriptional inhibition of *CCT5* following E7386 treatment.

Taken together, these results support our proposed causal model suggesting that cellular p-EMT phenotype is regulated downstream of β-catenin/CBP and mediated by *CCT5* expression (Fig. 2B).

β-catenin/CBP activity promotes features associated with p-EMT in murine OSCC

Since our in silico and molecular analyses identified mTORC1-S6K pathway as downstream of β-catenin/CBP signaling and that convergence of these signals were associated with p-EMT cell states, we set out to extend this finding in vivo by examining the effects of β-catenin/CBP inhibition on tumor development using the 4NQO carcinogen-induced mouse model of OSCC. As a well-established inducer of OSCC in murine models[26], 4NQO treatment drives progressive histopathological changes in murine oral epithelia that include hyperplasia, dysplasia, carcinoma in situ, and frank OSCC, which parallel human OSCC pathogenesis with similar mutational signatures[54]. H&E-based histological analysis of oral epithelia from 4NQO-induced OSCC revealed a substantial region of atypical exophytic papillary squamous cell carcinoma with distinct areas comprising both cohesive cells and unorganized discohesive cells (Fig. 5AI, 4NQO, *Areas 1 & 2, respectively*). Conversely, mice treated with 4NQO followed by a small molecule inhibitor of the β-catenin-CBP interaction, E7386, did not form OSCC but rather displayed regions of focal acanthosis and mild dysplasia pathology (Fig. 5AI, *4NQO + E7386, broken line boxed areas, top & bottom*).

Immunofluorescence staining of 4NQO-induced OSCC revealed that cohesive cell regions formed broad and punctate E-cadherin junctions and displayed diffuse cytoplasmic p-S6K staining with little detectable expression of a p-EMT marker, podoplanin (Fig. 5AII, *Area 1, arrow*). Regions of discohesive cells exhibited reduced punctate and poorly organized E-cadherin at cell-cell borders, with higher intensity of p-S6K localized to areas of robust podoplanin expression, indicating that these cells have lost epithelial characteristics (Fig. 5AII, *Area 2, arrow*). In contrast, oral epithelial tissues from mice treated with 4NQO and E7386 contained cells with well-organized and focused E-cadherin junctions, along with diffuse p-S6K and undetectable podoplanin staining (Fig. 5AII, 4NQO + E7386, *top boxed area*). Additionally, examination of a sagittal section of mild dysplasia revealed prominent E-cadherin cell-cell contacts, diminished p-S6K signal and podoplanin primarily localized to basal cells at the rete ridges and extending with diminished intensity to the differentiated spinous layer (Fig. 5AII, 4NQO + E7386, *bottom boxed area*). Quantification of immunofluorescence staining of podoplanin by comparative analysis using a mixed model to account for the image-level-variability confirmed that Podoplanin staining was significantly reduced in 4NQO + E7386 treated tissues (p-value = 0.016, t-statistic = −2.5, mean difference = −0.87 log (relative fluorescence intensity)) (Fig. 5B). Thus, the oncogenic role of β-catenin/CBP in OSCC extends to include the induction of cell plasticity by facilitating the p-EMT phenotype.

Discussion

In this study, we leveraged scRNAseq data of OSCC with a newly developed computational workflow, which identified the crosstalk between β-catenin/CBP and mTORC1 signaling as upstream drivers of the malignancy-associated p-EMT phenotype. In-silico analyses of transcriptomics and proteomics data predicted that mTORC1 activation occurs via the up-regulation of genes belonging to the TRiC complex, which is necessary for processing raptor and mLST8 proteins required for mTORC1 activation[25]. Our analyses suggest that this mechanism is a likely driver of p-EMT across multiple phenotypes, such as patient HPV status[55] and HNSCC molecular subtypes[37,56,57]. Subsequent experimental validation demonstrated that pharmacological inhibition of β-catenin/CBP in human OSCC cell lines decreased mTORC1 activity and reduced expression of TRiC component, CCT5, resulting in a reduced expression of p-EMT-associated genes. Furthermore, analysis of 4NQO-induced OSCC in the murine model of oral carcinogenesis confirmed a critical role for the β-catenin/CBP axis in the induction of p-EMT markers and progression to advanced oral tumors.

Our study reveals a direct causal relationship between β-catenin/CBP signaling and mTORC1 activity in the alteration of cellular states in head and neck cancer. On a mechanistic level, our finding that β-catenin/CBP activates mTORC1 via the regulation of components of the TRiC complex, such as CCT5, is distinct from relationships reported for β-catenin and mTOR in other cancers. For example, activation of mTORC1 by β-catenin in liver cancer has been shown to be mediated by glutamine synthetase expression[58].Furthermore, a reverse relationship was reported for intestinal cancer where mTORC1 was shown to suppress β-catenin signaling by down-regulating Wnt receptor, FZD[59]. Therefore, our data suggest distinct signaling networks connecting β-catenin and mTOR in head and neck cancer.

While β-catenin/CBP and mTORC1 have been independently implicated in the induction of EMT phenotypes in other tissues[60–66], and while independent associations of Wnt/β-catenin, β-catenin/CBP and mTORC1 with head and neck cancer aggressiveness have been described, our findings provide the first demonstration that activating mTORC1 via β-catenin/CBP signaling promotes p-EMT phenotypes in this malignancy.

Additional results highlighted by our analyses included a significant high activity of *miR-143/145* in the taxonomic subgroup J2, indicated by negative enrichment of *miR-143/145* targets, and by significant up-regulation of *CARMN*, which is the host gene of the *miR-143/145* cluster (Fig. 1A–C, Table 1). Interestingly, both our causal models also inferred inhibition of mTORC1 signaling by *miR-145*, with partial correlation estimates in the E7386 and ICG-001 models of −0.25 (FDR = 5.84E-20) and −0.19 (FDR = 3.87E-12), respectively (Fig. 2, Supplemental Table S4). The *miR-143/145* cluster has been previously described to target tumor-associated genes across many cancer types[67], including HNSCC[68–70], and *miR-145* has been shown to impede mTORC1 signaling through targeting S6K's encoding transcript, *RPS6KB1*, in colorectal cancer[71]. Taken together, these findings point to the *miR-143/145* cluster as another candidate mediator of mTORC1 activity, and a potential direction of investigation to be explored in future studies.

The functional in-vitro analyses were performed based on HSC3 and CAL27 cells. These were chosen because HSC3 are metastatic, poorly differentiated cell lines expressing both epithelial and mesenchymal markers, and sensitive to β-catenin/CBP inhibition[72–74]. CAL27 are non-metastatic, well-differentiated epithelial cells that do not express mesenchymal markers and are less sensitive to β-catenin/CBP inhibition, thus unlikely to undergo p-EMT[7,75]. For these reasons, we used both cell lines to evaluate the effect of β-catenin/CBP on mTORC1 and CCT5 (i.e., to evaluate the β-catenin/CBP ⇒ mTORC1 link of Fig. 2B), and only HSC3 to evaluate the effect of β-catenin/CBP through mTORC1 on p-EMT (i.e., the β-catenin/CBP ⇒ mTORC1 ⇒ p-EMT cascade of Fig. 2B).

We emphasize that these analyses were primarily aimed at generating insights into a focused group of cancer-related signaling pathways in head and neck cancer. Hence, these analyses were limited to 54 annotated gene sets we deemed most relevant to that aim, including cancer hallmarks[34,35], experimentally derived β-catenin/CBP gene sets[7], and targets of miRNAs, *miR-145* and *miR-143*[36]. Consequently, it is likely that these analyses do not capture the full repertoire of pathways contributing to cellular plasticity in head and neck cancer. However, while our in-silico model of causal interactions regulating head and neck cancer was non-exhaustive, our biochemical and molecular validation provided strong support for the model and subsequent findings presented.

In summary, this study applies an innovative computational workflow to the interrogation of scRNAseq data from HNSCC aimed to develop a more thorough understanding of the upstream drivers of the p-EMT phenotype in head and neck cancer. The finding that β-catenin/CBP activates mTORC1, which, in turn, is coupled to p-EMT phenotypes and associated with poor survival of head and neck cancer patients[10], underscores its importance as a key driver of tumor evolution and provides new information about additional *bona fide* therapeutic targets for this malignancy. Finally, this activation cascade emphasizes the potential of β-catenin/CBP inhibition as a promising head and neck cancer therapeutic intervention that distinctly targets more aggressive cells with elevated β-catenin/CBP activity[7]. Several Wnt/β-catenin inhibitors currently being investigated for their therapeutic potential, and multiple ongoing clinical trials, further attest to the translational significance of our findings[13].

Supplementary Material

Refer to Web version on PubMed Central for supplementary material.

Acknowledgements

We acknowledge the TCGA Research Network (https://www.cancer.gov/tcga) for granting access to cancer patient bulk expression data. We would like to thank David Sherr for his feedback on the interpretation of the study results.

This study was supported by NIH grants 5 R01 DE030350 (MAK, SM, XV), R01 DE030350 S1 (SM), R01 DE031831 (SM), R01 DE031413 (MVB), ACS Research Scholar Award RSG-17-138-01-CSM (XV), and Eisai Co., Ltd Research Award (MAK).

Trustees of Boston University (“Boston University”) and Eisai, Inc. (“Eisai”) have executed a Material Transfer Agreement (“MTA”) in which Maria Kukuruzinska is a named investigator and a Sponsored Research Agreement (“SRA”) in which Maria Kukuruzinska was the named principal investigator. All authors have read the journal’s authorship agreement and policy on disclosure of potential conflicts of interest.

Abbreviations

4NQO	4-nitroquinoline 1-oxide
ACTN1	Alpha-actinin-1
CBP	CREB-binding protein
CCLE	Cancer Cell Line Encyclopedia
CCT5	Chaperonin containing TCP1 subunit 5
CDF	chip definition file
CREB	cAMP-responsive element binding
CSC	cancer stem cell
DMSO	Dimethyl sulfoxide
EMT	epithelial-to-mesenchymal transition
FBS	fetal bovine serum
FDR	false discovery rate
GEO	Gene Expression Omnibus
GSEA	gene set enrichment analysis
GSVA	gene set variation analysis
H&E	Hematoxylin and eosin
HNSCC	head and neck squamous cell carcinoma
IACUC	Boston University's Institutional Animal Care & Use Committee
K2T	K2Taxonomer
LGALS1	Galectin 1
mSigDB	Molecular Signatures Database
mTORC1	mTOR Complex 1
OSCC	oral squamous cell carcinoma
p-EMT	partial epithelial-to-mesenchymal transition
p-S6K	phosphorylated S6K
PDPN	Podoplanin
RMA	robust multiarray average
RNAseq	RNA sequencing

RT	reverse transcriptase
RPPA	Reverse-phase protein array
RT-qPCR	reverse transcription quantitative polymerase chain reaction
scRNAseq	single-cell RNA sequencing
siRNA	small interfering RNA
TCGA	The Cancer Genome Atlas
TPM	transcripts-per-million counts
TRiC	T-complex protein ring complex

References

1. Kim HAJ, Zeng PYF, Shaikh MH, et al. All HPV-negative head and neck cancers are not the same:Analysis of the TCGA dataset reveals that anatomical sites have distinct mutation, transcriptome, hypoxia, and tumor microenvironment profiles. Oral Oncology. 2021;116:105260. doi:10.1016/j.oraloncology.2021.105260 [PubMed: 33725617]
2. Miller KD, Nogueira L, Mariotto AB, et al. Cancer treatment and survivorship statistics, 2019. CA A Cancer J Clin. 2019;69(5):363–385. doi:10.3322/caac.21565
3. Siegel RL, Miller KD, Fuchs HE, Jemal A. Cancer Statistics, 2021. CA A Cancer J Clin. 2021;71(1):7–33. doi:10.3322/caac.21654
4. Torborg SR, Li Z, Chan JE, Tammela T. Cellular and molecular mechanisms of plasticity in cancer. Trends in Cancer. 2022;8(9):735–746. doi:10.1016/j.trecan.2022.04.007 [PubMed: 35618573]
5. LaFave LM, Kartha VK, Ma S, et al. Epigenomic State Transitions Characterize Tumor Progression in Mouse Lung Adenocarcinoma. Cancer Cell. 2020;38(2):212–228.e13. doi:10.1016/j.ccell.2020.06.006 [PubMed: 32707078]
6. Marjanovic ND, Hofree M, Chan JE, et al. Emergence of a High-Plasticity Cell State during Lung Cancer Evolution. Cancer Cell. 2020;38(2):229–246.e13. doi:10.1016/j.ccell.2020.06.012 [PubMed: 32707077]
7. Kartha VK, Alamoud KA, Sadykov K, et al. Functional and genomic analyses reveal therapeutic potential of targeting β-catenin/CBP activity in head and neck cancer. Genome Med. 2018;10(1):54. doi:10.1186/s13073-018-0569-7 [PubMed: 30029671]
8. Beane JE, Mazzilli SA, Campbell JD, et al. Molecular subtyping reveals immune alterations associated with progression of bronchial premalignant lesions. Nat Commun. 2019;10(1):1856. doi:10.1038/s41467-019-09834-2 [PubMed: 31015447]
9. Parikh AS, Puram SV, Faquin WC, et al. Immunohistochemical quantification of partial-EMT in oral cavity squamous cell carcinoma primary tumors is associated with nodal metastasis. Oral Oncol. 2019;99:104458. doi:10.1016/j.oraloncology.2019.104458 [PubMed: 31704557]
10. Puram SV, Tirosh I, Parikh AS, et al. Single-Cell Transcriptomic Analysis of Primary and Metastatic Tumor Ecosystems in Head and Neck Cancer. Cell. 2017;171(7):1611–1624.e24. doi:10.1016/j.cell.2017.10.044 [PubMed: 29198524]
11. Tada H, Takahashi H, Ida S, Nagata Y, Chikamatsu K. Epithelial-Mesenchymal Transition Status of Circulating Tumor Cells Is Associated With Tumor Relapse in Head and Neck Squamous Cell Carcinoma. Anticancer Res. 2020;40(6):3559–3564. doi:10.21873/anticanres.14345 [PubMed: 32487658]
12. Wan Y, Liu H, Zhang M, et al. Prognostic value of epithelial-mesenchymal transition-inducing transcription factors in head and neck squamous cell carcinoma: A meta-analysis. Head Neck. 2020;42(5):1067–1076. doi:10.1002/hed.26104 [PubMed: 32048783]

13. Alamoud KA, Kukuruzinska MA. Emerging Insights into Wnt/β-catenin Signaling in Head and Neck Cancer. J Dent Res. 2018;97(6):665–673. doi:10.1177/0022034518771923 [PubMed: 29771197]
14. Fodde R, Brabletz T. Wnt/β-catenin signaling in cancer stemness and malignant behavior. Current Opinion in Cell Biology. 2007;19(2):150–158. doi:10.1016/j.ceb.2007.02.007 [PubMed: 17306971]
15. Holland JD, Klaus A, Garratt AN, Birchmeier W. Wnt signaling in stem and cancer stem cells. Current Opinion in Cell Biology. 2013;25(2):254–264. doi:10.1016/j.ceb.2013.01.004 [PubMed: 23347562]
16. Lee SH, Koo BS, Kim JM, et al. Wnt/β-catenin signalling maintains self-renewal and tumourigenicity of head and neck squamous cell carcinoma stem-like cells by activating Oct4. J Pathol. 2014;234(1):99–107. doi:10.1002/path.4383 [PubMed: 24871033]
17. Ma H, Nguyen C, Lee KS, Kahn M. Differential roles for the coactivators CBP and p300 on TCF/β-catenin-mediated survivin gene expression. Oncogene. 2005;24(22):3619–3631. doi:10.1038/sj.onc.1208433 [PubMed: 15782138]
18. Song J, Chang I, Chen Z, Kang M, Wang CY. Characterization of Side Populations in HNSCC: Highly Invasive, Chemoresistant and Abnormal Wnt Signaling. Huang S, ed. PLoS ONE. 2010;5(7):e11456. doi:10.1371/journal.pone.0011456 [PubMed: 20625515]
19. Spranger S, Gajewski TF. A new paradigm for tumor immune escape: β-catenin-driven immune exclusion. j immunotherapy cancer. 2015;3(1):43. doi:10.1186/s40425-015-0089-6
20. Spranger S, Bao R, Gajewski TF. Melanoma-intrinsic β-catenin signalling prevents anti-tumour immunity. Nature. 2015;523(7559):231–235. doi:10.1038/nature14404 [PubMed: 25970248]
21. Wend P, Fang L, Zhu Q, et al. Wnt/β-catenin signalling induces MLL to create epigenetic changes in salivary gland tumours. EMBO J. 2013;32(14):1977–1989. doi:10.1038/emboj.2013.127 [PubMed: 23736260]
22. Yang K, Wang X, Zhang H, et al. The evolving roles of canonical WNT signaling in stem cells and tumorigenesis: implications in targeted cancer therapies. Lab Invest. 2016;96(2):116–136. doi:10.1038/labinvest.2015.144 [PubMed: 26618721]
23. Chandler KB, Alamoud KA, Stahl VL, et al. β-Catenin/CBP inhibition alters epidermal growth factor receptor fucosylation status in oral squamous cell carcinoma. Mol Omics. 2020;16(3):195–209. doi:10.1039/D0MO00009D [PubMed: 32203567]
24. Yamada K, Hori Y, Inoue S, et al. E7386, a Selective Inhibitor of the Interaction between β-Catenin and CBP, Exerts Antitumor Activity in Tumor Models with Activated Canonical Wnt Signaling. Cancer Res. 2021;81(4):1052–1062. doi:10.1158/0008-5472.CAN-20-0782 [PubMed: 33408116]
25. Cuéllar J, Ludlam WG, Tensmeyer NC, et al. Structural and functional analysis of the role of the chaperonin CCT in mTOR complex assembly. Nat Commun. 2019;10(1):2865. doi:10.1038/s41467-019-10781-1 [PubMed: 31253771]
26. Osei-Sarfo K, Tang XH, Urvalek AM, Scognamiglio T, Gudas LJ. The molecular features of tongue epithelium treated with the carcinogen 4-nitroquinoline-1-oxide and alcohol as a model for HNSCC. Carcinogenesis. 2013;34(11):2673–2681. doi:10.1093/carcin/bgt223 [PubMed: 23784083]
27. Benjamini Y, Hochberg Y. Controlling the false discovery rate: a practical and powerful approach to multiple testing. Journal of the Royal Statistical Society: Series B (Methodological). 1995;57(1):289–300. doi:10.1111/j.2517-6161.1995.tb02031.x
28. Gautier L, Cope L, Bolstad BM, Irizarry RA. affy--analysis of Affymetrix GeneChip data at the probe level. Bioinformatics. 2004;20(3):307–315. doi:10.1093/bioinformatics/btg405 [PubMed: 14960456]
29. Ritchie ME, Phipson B, Wu D, et al. limma powers differential expression analyses for RNA-sequencing and microarray studies. Nucleic Acids Research. 2015;43(7):e47–e47. doi:10.1093/nar/gkv007 [PubMed: 25605792]
30. Stuart T, Butler A, Hoffman P, et al. Comprehensive integration of single-cell data. Cell. 2019;177(7):1888–1902.e21. doi:10.1016/j.cell.2019.05.031 [PubMed: 31178118]

31. Reed ER, Monti S. Multi-resolution characterization of molecular taxonomies in bulk and single-cell transcriptomics data. Nucleic Acids Research. Published online July 6, 2021:gkab552. doi:10.1093/nar/gkab552
32. Wagstaff K, Cardie C, Rogers S, Schrödl S. Constrained K-means clustering with background knowledge. In: ICML. ; 2001:577–584.
33. Hänzelmann S, Castelo R, Guinney J. GSVA: gene set variation analysis for microarray and RNA-Seq data. BMC Bioinformatics. 2013;14(1):7. doi:10.1186/1471-2105-14-7 [PubMed: 23323831]
34. Subramanian A, Tamayo P, Mootha VK, et al. Gene set enrichment analysis: A knowledge-based approach for interpreting genome-wide expression profiles. Proceedings of the National Academy of Sciences. 2005;102(43):15545–15550. doi:10.1073/pnas.0506580102
35. Liberzon A, Subramanian A, Pinchback R, Thorvaldsdottir H, Tamayo P, Mesirov JP. Molecular signatures database (MSigDB) 3.0. Bioinformatics. 2011;27(12):1739–1740. doi:10.1093/bioinformatics/btr260 [PubMed: 21546393]
36. Daina A, Michielin O, Zoete V. SwissTargetPrediction: updated data and new features for efficient prediction of protein targets of small molecules. Nucleic Acids Research. 2019;47(W1):W357–W364. doi:10.1093/nar/gkz382 [PubMed: 31106366]
37. The Cancer Genome Atlas Network. Comprehensive genomic characterization of head and neck squamous cell carcinomas. Nature. 2015;517(7536):576–582. doi:10.1038/nature14129 [PubMed: 25631445]
38. Robinson MD, McCarthy DJ, Smyth GK. edgeR: a Bioconductor package for differential expression analysis of digital gene expression data. Bioinformatics. 2010;26(1):139–140. doi:10.1093/bioinformatics/btp616 [PubMed: 19910308]
39. Spirtes P, Glymour C. An Algorithm for Fast Recovery of Sparse Causal Graphs. Social Science Computer Review. 1991;9(1):62–72. doi:10.1177/089443939100900106
40. Kalisch M, Mächler M, Colombo D, Maathuis MH, Bühlmann P. Causal Inference Using Graphical Models with the *R* Package **pcalg**. J Stat Soft. 2012;47(11). doi:10.18637/jss.v047.i11
41. Greenland S Quantifying biases in causal models: classical confounding vs collider-stratification bias. Epidemiology. 2003;14(3):300–306. [PubMed: 12859030]
42. Fonseca BD, Zakaria C, Jia JJ, et al. La-related Protein 1 (LARP1) Represses Terminal Oligopyrimidine (TOP) mRNA Translation Downstream of mTOR Complex 1 (mTORC1). J Biol Chem. 2015;290(26):15996–16020. doi:10.1074/jbc.M114.621730 [PubMed: 25940091]
43. Ghandi M, Huang FW, Jané-Valbuena J, et al. Next-generation characterization of the Cancer Cell Line Encyclopedia. Nature. 2019;569(7757):503–508. doi:10.1038/s41586-019-1186-3 [PubMed: 31068700]
44. Colaprico A, Silva TC, Olsen C, et al. TCGAbiolinks: an R/Bioconductor package for integrative analysis of TCGA data. Nucleic Acids Research. 2016;44(8):e71–e71. doi:10.1093/nar/gkv1507 [PubMed: 26704973]
45. Silva TC, Colaprico A, Olsen C, et al. TCGA Workflow: Analyze cancer genomics and epigenomics data using Bioconductor packages. F1000Res. 2016;5:1542. doi:10.12688/f1000research.8923.2 [PubMed: 28232861]
46. Mounir M, Lucchetta M, Silva TC, et al. New functionalities in the TCGAbiolinks package for the study and integration of cancer data from GDC and GTEx. Wang E, ed. PLoS Comput Biol. 2019;15(3):e1006701. doi:10.1371/journal.pcbi.1006701 [PubMed: 30835723]
47. Yoshihara K, Shahmoradgoli M, Martínez E, et al. Inferring tumour purity and stromal and immune cell admixture from expression data. Nat Commun. 2013;4(1):2612. doi:10.1038/ncomms3612 [PubMed: 24113773]
48. Li J, Zhao W, Akbani R, et al. Characterization of Human Cancer Cell Lines by Reverse-phase Protein Arrays. Cancer Cell. 2017;31(2):225–239. doi:10.1016/j.ccell.2017.01.005 [PubMed: 28196595]
49. Schneider CA, Rasband WS, Eliceiri KW. NIH Image to ImageJ: 25 years of image analysis. Nat Methods. 2012;9(7):671–675. doi:10.1038/nmeth.2089 [PubMed: 22930834]
50. Kuznetsova A, Brockhoff PB, Christensen RHB. **lmerTest** Package: Tests in Linear Mixed Effects Models. J Stat Soft. 2017;82(13). doi:10.18637/jss.v082.i13

51. Kawasaki G, Naruse T, Furukawa K, Umeda M. mTORC1 and mTORC2 Expression Levels in Oral Squamous Cell Carcinoma: An Immunohistochemical and Clinicopathological Study. Anticancer Res. 2018;38(3):1623–1628. doi:10.21873/anticanres.12393 [PubMed: 29491094]
52. Yu CC, Hung SK, Lin HY, et al. Targeting the PI3K/AKT/mTOR signaling pathway as an effectively radiosensitizing strategy for treating human oral squamous cell carcinoma *in vitro* and *in vivo*. Oncotarget. 2017;8(40):68641–68653. doi:10.18632/oncotarget.19817 [PubMed: 28978144]
53. Zeng L, Fagotto F, Zhang T, et al. The Mouse Fused Locus Encodes Axin, an Inhibitor of the Wnt Signaling Pathway That Regulates Embryonic Axis Formation. Cell. 1997;90(1):181–192. doi:10.1016/S0092-8674(00)80324-4 [PubMed: 9230313]
54. Haddad RI, Shin DM. Recent Advances in Head and Neck Cancer. N Engl J Med. 2008;359(11):1143–1154. doi:10.1056/NEJMra0707975 [PubMed: 18784104]
55. Kobayashi K, Hisamatsu K, Suzui N, Hara A, Tomita H, Miyazaki T. A Review of HPV-Related Head and Neck Cancer. JCM. 2018;7(9):241. doi:10.3390/jcm7090241 [PubMed: 30150513]
56. Chung CH, Parker JS, Karaca G, et al. Molecular classification of head and neck squamous cell carcinomas using patterns of gene expression. Cancer Cell. 2004;5(5):489–500. doi:10.1016/S1535-6108(04)00112-6 [PubMed: 15144956]
57. Walter V, Yin X, Wilkerson MD, et al. Molecular Subtypes in Head and Neck Cancer Exhibit Distinct Patterns of Chromosomal Gain and Loss of Canonical Cancer Genes. Teh MT, ed. PLoS ONE. 2013;8(2):e56823. doi:10.1371/journal.pone.0056823 [PubMed: 23451093]
58. Adebayo Michael AO, Ko S, Tao J, et al. Inhibiting Glutamine-Dependent mTORC1 Activation Ameliorates Liver Cancers Driven by β-Catenin Mutations. Cell Metabolism. 2019;29(5):1135–1150.e6. doi:10.1016/j.cmet.2019.01.002 [PubMed: 30713111]
59. Zeng H, Lu B, Zamponi R, et al. mTORC1 signaling suppresses Wnt/β-catenin signaling through DVL-dependent regulation of Wnt receptor FZD level. Proc Natl Acad Sci USA. 2018;115(44):E10362–E10369. doi:10.1073/pnas.1808575115 [PubMed: 30297426]
60. Kim WK, Kwon Y, Jang M, et al. β-catenin activation down-regulates cell-cell junction-related genes and induces epithelial-to-mesenchymal transition in colorectal cancers. Sci Rep. 2019;9(1):18440. doi:10.1038/s41598-019-54890-9 [PubMed: 31804558]
61. Song Y, Li Z xia, Liu X, Wang R, Li L wei, Zhang Q. The Wnt/β-catenin and PI3K/Akt signaling pathways promote EMT in gastric cancer by epigenetic regulation via H3 lysine 27 acetylation. Tumour Biol. 2017;39(7):101042831771261. doi:10.1177/1010428317712617
62. Jiang YG, Luo Y, He D lin, et al. Role of Wnt/β-catenin signaling pathway in epithelial-mesenchymal transition of human prostate cancer induced by hypoxia-inducible factor-1α: Prostate cancer undergoes EMT via Wnt. International Journal of Urology. 2007;14(11):1034–1039. doi:10.1111/j.1442-2042.2007.01866.x [PubMed: 17956532]
63. Henderson WR, Chi EY, Ye X, et al. Inhibition of Wnt/ -catenin/CREB binding protein (CBP) signaling reverses pulmonary fibrosis. Proceedings of the National Academy of Sciences. 2010;107(32):14309–14314. doi:10.1073/pnas.1001520107
64. Lamouille S, Connolly E, Smyth JW, Akhurst RJ, Derynck R. TGF-β-induced activation of mTOR complex 2 drives epithelial–mesenchymal transition and cell invasion. Journal of Cell Science. 2012;125(5):1259–1273. doi:10.1242/jcs.095299 [PubMed: 22399812]
65. Gulhati P, Bowen KA, Liu J, et al. mTORC1 and mTORC2 Regulate EMT, Motility, and Metastasis of Colorectal Cancer via RhoA and Rac1 Signaling Pathways. Cancer Res. 2011;71(9):3246–3256. doi:10.1158/0008-5472.CAN-10-4058 [PubMed: 21430067]
66. Saito M, Mitani A, Ishimori T, et al. Active mTOR in Lung Epithelium Promotes Epithelial–Mesenchymal Transition and Enhances Lung Fibrosis. Am J Respir Cell Mol Biol. 2020;62(6):699–708. doi:10.1165/rcmb.2019-0255OC [PubMed: 32208980]
67. Das AV, Pillai RM. Implications of miR cluster 143/145 as universal anti-oncomiRs and their dysregulation during tumorigenesis. Cancer Cell Int. 2015;15(1):92. doi:10.1186/s12935-015-0247-4 [PubMed: 26425114]
68. Yamada Y, Koshizuka K, Hanazawa T, et al. Passenger strand of miR-145–3p acts as a tumor-suppressor by targeting MYO1B in head and neck squamous cell carcinoma. Int J Oncol. Published online November 6, 2017. doi:10.3892/ijo.2017.4190

69. Zhang J, Sun Q, Zhang Z, Ge S, Han ZG, Chen WT. Loss of microRNA-143/145 disturbs cellular growth and apoptosis of human epithelial cancers by impairing the MDM2-p53 feedback loop. Oncogene. 2013;32(1):61–69. doi:10.1038/onc.2012.28 [PubMed: 22330136]

70. Peschiaroli A, Giacobbe A, Formosa A, et al. miR-143 regulates hexokinase 2 expression in cancer cells. Oncogene. 2013;32(6):797–802. doi:10.1038/onc.2012.100 [PubMed: 22469988]

71. Xu Q, Liu LZ, Qian X, et al. MiR-145 directly targets p70S6K1 in cancer cells to inhibit tumor growth and angiogenesis. Nucleic Acids Research. 2012;40(2):761–774. doi:10.1093/nar/gkr730 [PubMed: 21917858]

72. Momose F, Araida T, Negishi A, Ichijo H, Shioda S, Sasaki S. Variant sublines with different metastatic potentials selected in nude mice from human oral squamous cell carcinomas. J Oral Pathol Med. 1989;18(7):391–395. doi:10.1111/j.1600-0714.1989.tb01570.x [PubMed: 2585303]

73. Tanaka M, Harada H, Kimura H. The role of H3K9me3 in oral squamous cell carcinoma. Biochemical and Biophysical Research Communications. 2023;640:56–63. doi:10.1016/j.bbrc.2022.11.102 [PubMed: 36502632]

74. Moriwaki K, Ayani Y, Kuwabara H, Terada T, Kawata R, Asahi M. TRKB tyrosine kinase receptor is a potential therapeutic target for poorly differentiated oral squamous cell carcinoma. Oncotarget. 2018;9(38):25225–25243. doi:10.18632/oncotarget.25396 [PubMed: 29861866]

75. Bais MV, Kukuruzinska M, Trackman PC. Orthotopic non-metastatic and metastatic oral cancer mouse models. Oral Oncology. 2015;51(5):476–482. doi:10.1016/j.oraloncology.2015.01.012 [PubMed: 25682387]

Brief Commentary

Background

Despite advances in characterizing genomic alterations in head and neck cancers, targeted therapies remain elusive, and these malignancies continue to rank among the deadliest cancers. Growing evidence has indicated that cell plasticity, including the loss of the epithelial state, contributes to cancer initiation and the progression to aggressive disease. To develop rational targeted therapies, a better mechanistic understanding of molecular signaling and their contribution to intra-tumor phenotypes is needed. To this end, we implemented an analytical workflow integrating scRNAseq profiles from human oral squamous cell carcinomas (OSCC) with bulk transcriptomics and proteomics data from multiple public head and neck cancer repositories, devised to characterize co-activated pathways and cell states in tumor cell clusters and elucidate causal relationships. Our analyses revealed activation of mTORC1 by β-catenin/CBP as an upstream driver of the partial epithelial-mesenchymal transition (p-EMT), associated with aggressive OSCC features. Targeted validation experiments supported these findings.

Translational Significance

The identification of β-catenin/CBP-mTORC1-pEMT cascade highlights β-catenin/CBP as a key driver of OSCC and potential bona fide therapeutic target.

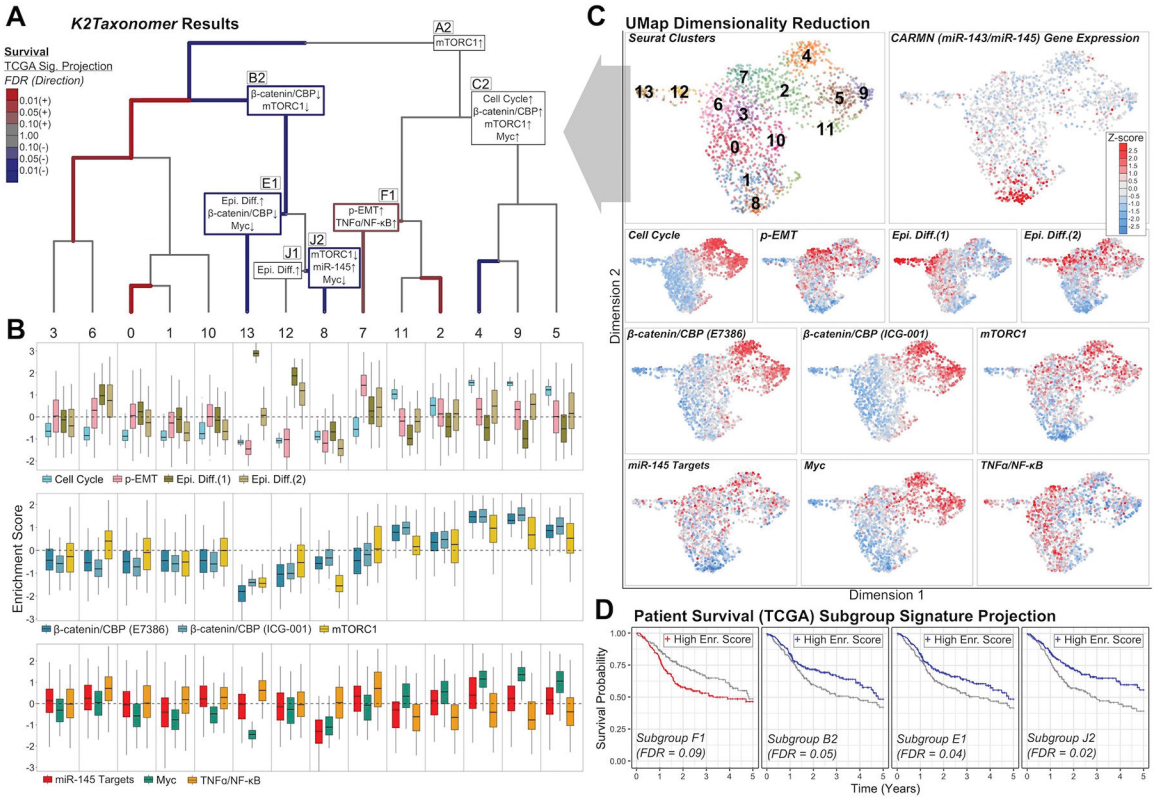

Figure 1: Characterization of Signatures of Head and Neck Cancer Cells from scRNAseq Data

A. K2T derived subgroups of scRNAseq cell clusters. Subgroups are labeled with a letter and digit, with the letter indicating the specific partition in the taxonomy and the digits, 1 or 2, indicating the left and right subgroups split at that partition, respectively. Top pathways/cell states and labels for selected segments are given. The set of statistical results for these pathways are shown in Table 1. Colored segments indicate associations between signatures derived from each subgroup and survival in TCGA HNSCC bulk expression data. Red and blue segments indicate statistically significant (FDR < 0.1) associations with hazard ratios greater or less than 1, respectively, i.e., worse or better patient survival. The full set of survival analyses results are shown in Table 2.

B. Distributions of GSVA-based enrichments scores for top pathways/cell states shown in Fig. 1A. Differential enrichment results for selected subgroups are shown in Table 1.

C. UMAP representation of the scRNAseq data, representing cell cluster identities, expression of *CARMN*, and top pathways/cell states shown in Fig. 1A.

D. Kaplan-Meier visualization of subgroup signatures associated with TCGA HNSCC patients' survival. Each curve represents patients in the top and bottom 40th percentiles of enrichment scores of each signature. Colored curves indicate which curve represents the top 40th percentile group, i.e., patients with the highest enrichment scores. The colors, red and blue, indicate whether these higher enrichment scores were associated with hazard ratios greater or less than 1, respectively, based on Cox proportional hazards testing. Likewise, the FDR values are derived from Cox proportional hazards testing as well. The full set of survival analyses results are shown in Table 2.

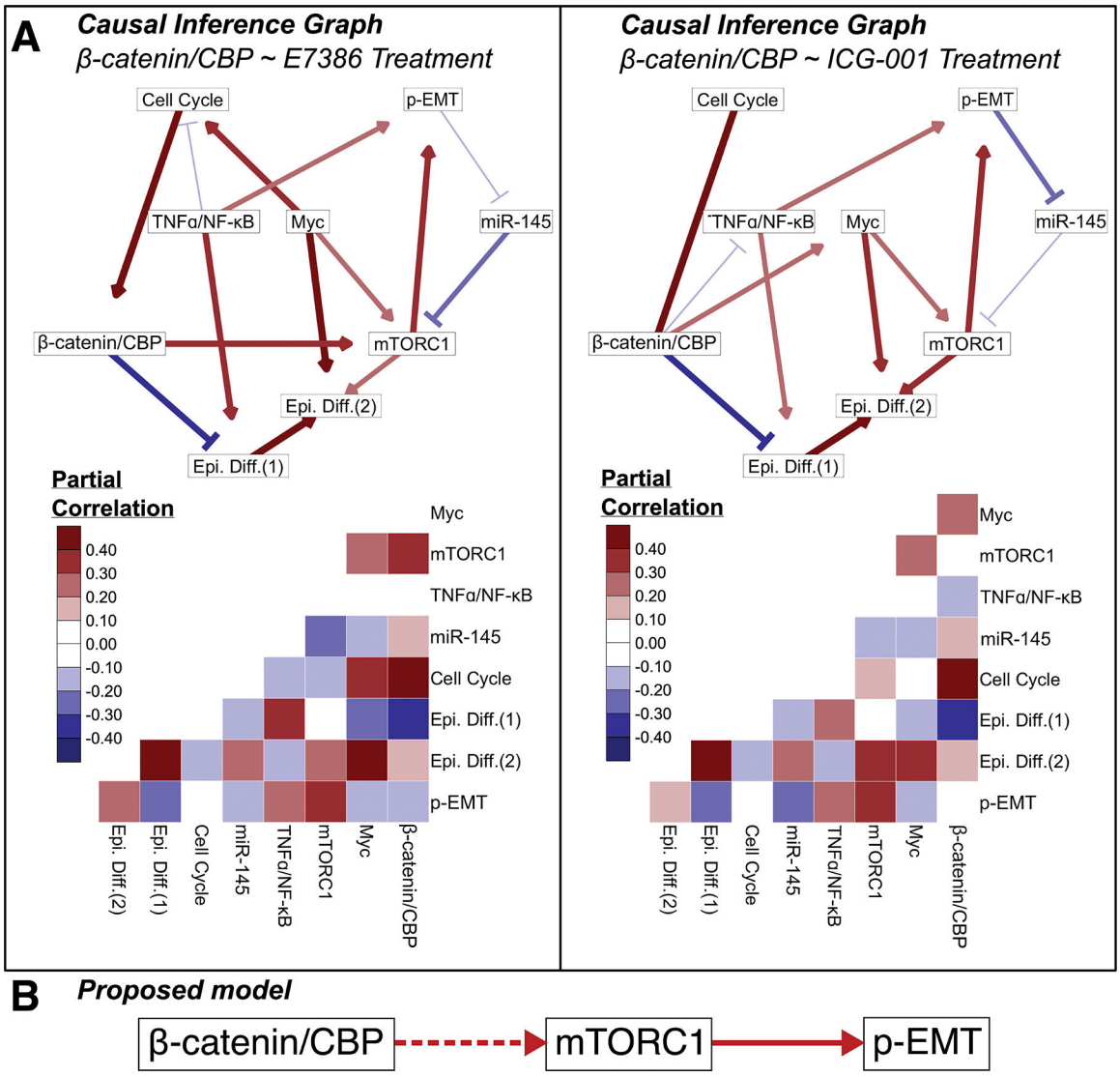

Figure 2: Causal Inference Models of Interactions Between Pathways/Cell States in Head and Neck Cancer scRNAseq Data

A. Causal inference graphs indicated inferred causal relationships of pathways and cell states. The right and left graphs represent separate causal models including separate β-catenin/CBP gene sets, derived from either E7386 or ICG001 treatments, respectively. Partial correlation estimate maps are shown below each graph. The color scale for the vertices in the causal inference are in concordance with the partial correlation estimates. The full set of results for partial correlation and causal inference analysis are shown in Supplemental Table S4.

B. Proposed causal model of mTORC1 activation by β–catenin/CBP upstream of induction p-EMT. The dashed line indicates that mTORC1 activation of β–catenin/CBP may be direct and/or mediated by Myc.

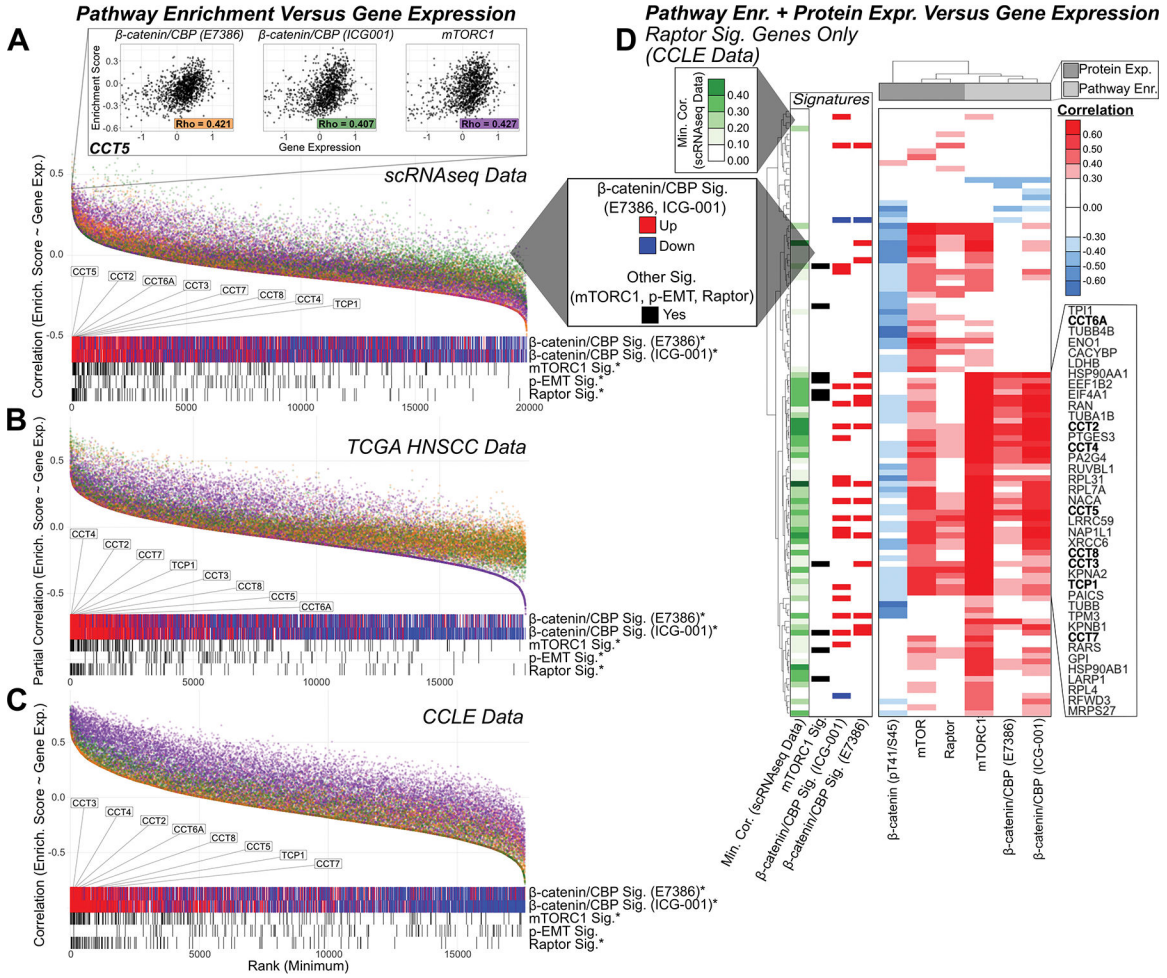

Figure 3: Functional Analysis Identifying Transcriptional Mediators Between β-catenin/CBP and mTORC1 Signaling

Functional analysis comparing gene expression to enrichment scores of β-catenin/CBP and mTORC1 signaling and protein expression for both scRNAseq and CCLE cell line data. A. Rank-based analyses of comparisons of correlation between the expression of genes in the scRNAseq data and GSVA-based enrichment scores for each of the three total β-catenin/CBP and mTORC1 gene sets. Genes are ranked according to their minimum correlation across all three analyses. Members of each of these signatures are shown below these rankings, as well as p-EMT markers and genes encoding raptor binding proteins. β-catenin/CBP geneset members are split into two groups based on whether they are up- or down-regulated by β-catenin/CBP, denoted by red and blue, respectively. Gene sets that are significantly enriched (FDR < 0.05) based on pre-ranked GSEA are indicated by "*" to the right of their respective label. The top gene, most highly correlated with both β-catenin/CBP and mTORC1, *CCT5*, is shown above the ranking plot. The position of TRiC complex genes, including *CCT5*, are labeled. The full set of pre-ranked GSEA analysis results are shown in Table 3.

B. Repeated analyses of (A) but performed on the TCGA HNSCC bulk expression data for primary tumor samples. Additional results of sample subsets stratified by HPV status and

HPV- gene expression subtypes are shown in Supplemental Fig. S1 and Supplemental Table S6.

C. Repeated analyses of (A) but performed on the CCLE cell line data.

D. Heatmap showing the correlation of expression of genes encoding raptor binding proteins across GSVA-based enrichment scores and protein expression in CCLE cell line data. “Min. Cor.” denotes the minimum correlation of these genes shown in (B). A subset of these genes that are consistently correlated with each enrichment score and protein expression are labeled to the right of the heatmap. TRiC complex genes within this subset are shown in boldface.

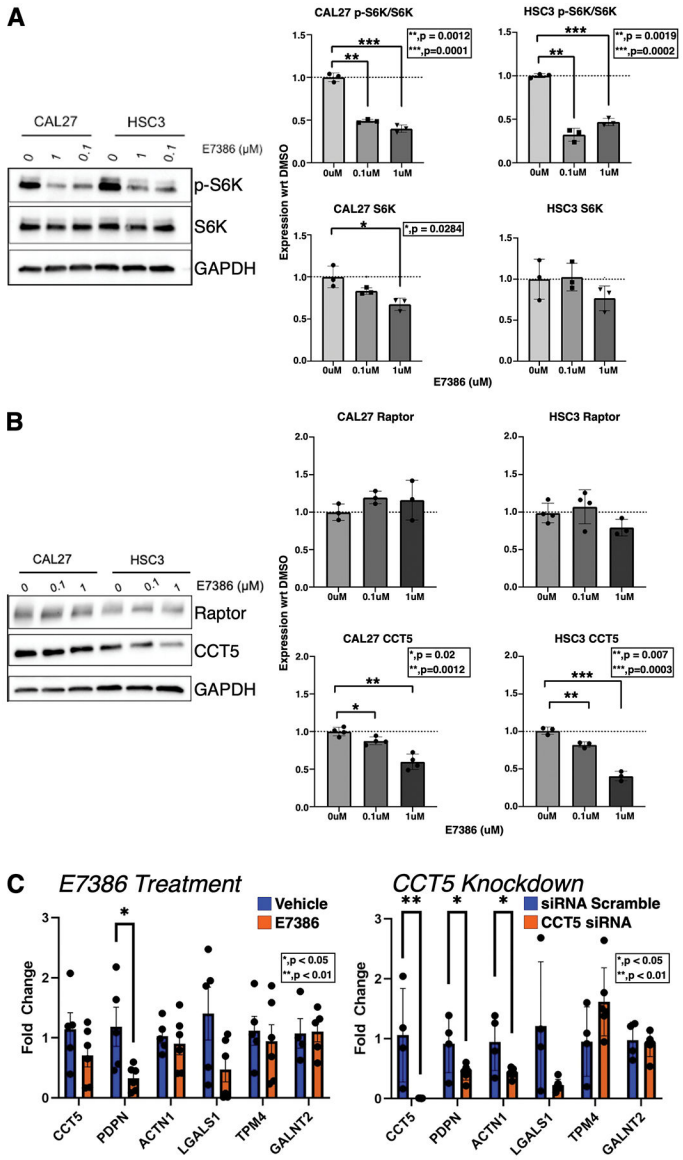

Figure 4: β-catenin/CBP Promotes mTORC1, CCT5, and p-EMT Phenotype in Human OSCC cell lines

A. Immunoblot experiments of S6K and p-S6K in CAL27 and HSC3 cells, following pharmacological knockdown of β-catenin/CBP with E7386 were conducted. The top and bottom rows of plots report the statistical results of measuring the ratios of p-S6K to total S6K and total S6K to GAPDH, respectively. Statistically significant results (p-value < 0.05) are marked with "*"s. The full set of statistical results are shown in Supplemental Table S7. An image of the gel representing one of the three replicates in this experiment is shown to the left, and images for each of the three replicates shown in Supplemental Fig. S2A.

B. Immunoblots examining raptor and CCT5 in CAL27 and HSC3 cells following pharmacological knockdown of β-catenin/CBP with E7386. The top and bottom rows of plots report the statistical results of measuring the ratios of raptor to GAPDH and CCT5 to GAPDH, respectively. Statistically significant results (p-value < 0.05) are marked with "*"s. The full set of statistical results are shown in Supplemental Table S7. An image of the gel

representing one of the four replicates in this experiment is shown to the left, and images for each of the four replicates shown in Supplemental Fig. S2B.

C. RT-qPCR experiments of changes in gene expression in HSC3 cells, following either pharmacological knockdown of β-catenin/CBP with E7386 (left) or siRNA mediated knockdown of CCT5. Evaluated genes include CCT5, as well as five p-EMT marker genes. Statistically significant results (p-value < 0.05) are marked with "*"s. The full set of statistical results are shown in Supplemental Table S8.

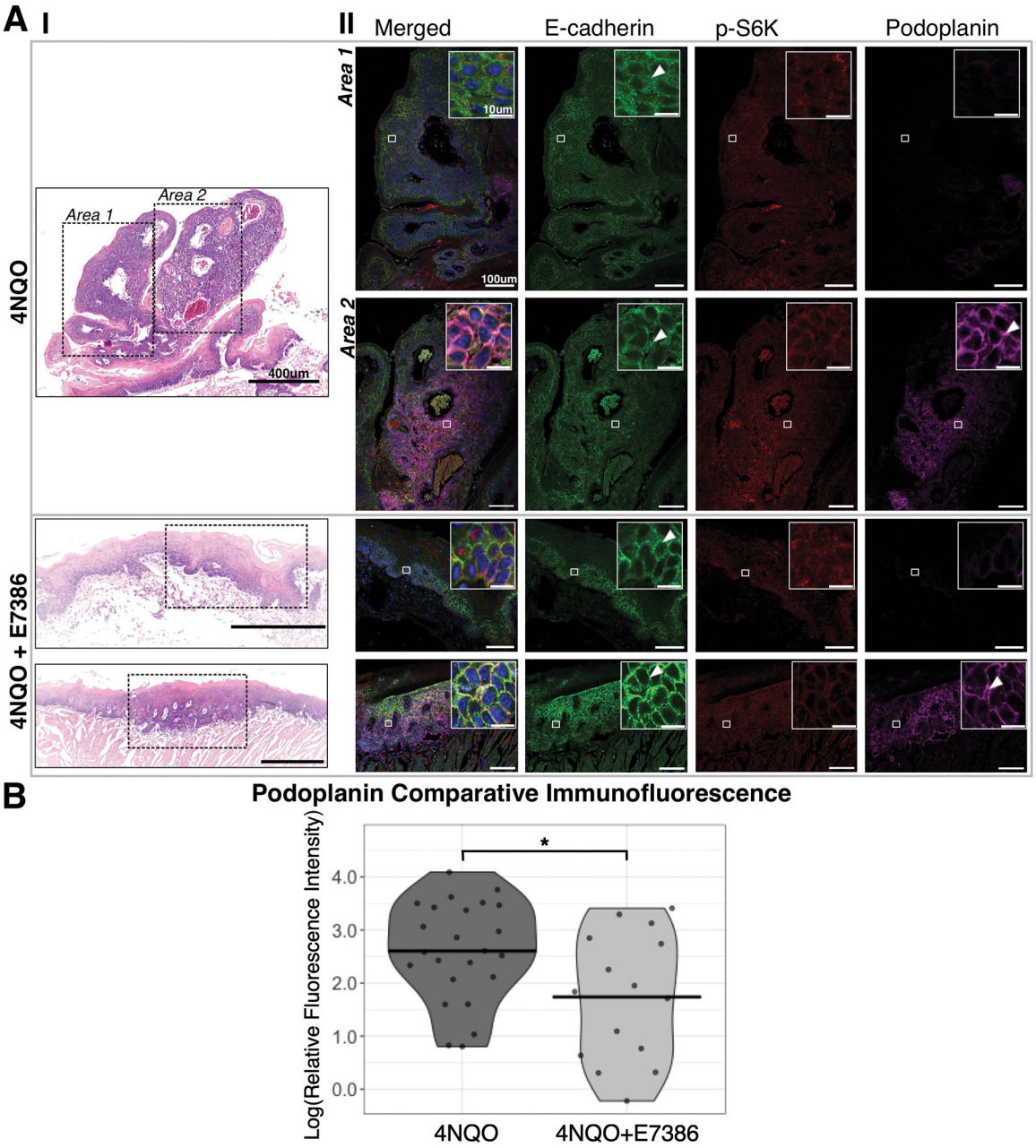

Figure 5. β-catenin/CBP Promotes p-EMT Phenotype in a 4NQO Murine Model of OSCC

A. I. H&E analysis of oral tongue lesions from 4NQO- and 4NQO + E7386-treated mice. Top panel depicts 4NQO-induced exophytic papillary squamous cell carcinoma comprising cohesive cells (*Area 1*) and disorganized discohesive cells (*Area 2*). The two bottom panels show the inhibitory effects of E7386 on 4NQO-induced OSCC development, with oral epithelia comprising regions of focal acanthosis and mild dysplasia pathology.

A. II. Immunofluorescence imaging of cell populations in 4NQO- and 4NQO + E7386-treated oral lesions. *Area 1* OSCC cells featured broad and punctate E-cadherin junctions associated with diffuse cytoplasmic p-S6K and low podoplanin signal (*small & blow-up large box, arrow*). *Area 2* comprised cells with punctate E-cadherin junctions but with

reduced signal, and displaying higher intensity p-S6K co-localized with a prominent podoplanin signal (*small & blow-up large boxes, arrow*). Oral epithelia from 4NQO + E7386 treated mice displayed regions of mild dysplasia containing cells with well-organized E-cadherin junctions, diffuse p-S6K and undetectable podoplanin signal (*Top boxed area, small & blow-up boxes, arrow*). Sagittal section revealed cells with well-organized E-cadherin cell-contacts, reduced p-S6K and podoplanin signal detected mostly in basal cells of rete ridges, extending into the spinous layer with diminishing intensity (*Bottom boxed area, small & blow-up boxes, arrow*).

B. Comparison of podoplanin immunofluorescence signals between from 4NQO + E7386 and 4NQO from multiple images per sample. The violin plot shows the distribution (points) and mean (horizontal lines) of the mean aggregated log(relative immunofluorescence signals) for each image. The statistically significant difference (p-value = 0.016) is indicated with “*”.

Table 1:

Differential Pathway/Cell state Enrichment Results for Selected Subgroups

Subgroup	Clusters	Pathway/Cell State	Difference	Mean Enrichment Score	T-score	P-value	FDR	Source
A2	7, 11, 2, 4, 9, 5	mTORC1 Signaling	0.17	−0.04	18.88	1.56E-72	7.33E-71	*a*
B2	13, 12, 8	β-catenin/CBP (E7386)	−0.08	−0.12	−7.30	5.95E-13	3.53E-12	*b*
		mTORC1 Signaling	−0.19	−0.11	−12.70	2.20E-34	4.75E-33	*a*
C2	4, 9, 5	Cell Cycle	0.48	0.34	26.78	1.65E-111	1.13E-109	*d*
		β-catenin/CBP (ICG001)	0.24	0.21	22.97	7.40E-89	4.29E-87	*c*
		β-catenin/CBP (E7386)	0.19	0.12	20.76	4.83E-76	2.43E-74	*b*
		mTORC1 Signaling	0.11	0.06	8.08	2.49E-15	1.69E-14	*a*
		Myc Signaling	0.21	0.16	13.85	4.87E-39	1.27E-37	*a*
E1	13	Epithelial Differentiation 1	0.61	0.16	11.68	9.38E-24	1.20E-22	*d*
		β-catenin/CBP (E7386)	−0.23	−0.18	−9.71	3.70E-18	3.25E-17	*b*
		β-catenin/CBP (ICG001)	−0.22	−0.17	−8.20	4.52E-14	2.96E-13	*b*
		Myc Signaling	−0.18	−0.28	−4.97	1.57E-06	4.81E-06	*a*
F1	7	p-EMT	0.30	0.08	13.65	2.89E-34	6.05E-33	*d*
		TNFα/NFκB	0.21	−0.05	11.33	1.58E-25	2.25E-24	*a*
J1	12	Epithelial Differentiation 2	0.66	−0.18	22.91	1.88E-49	7.87E-48	*d*
		Epithelial Differentiation 1	0.57	0.03	20.84	6.00E-45	2.16E-43	*d*
J2	8	mTORC1 Signaling	−0.21	−0.26	−7.92	6.26E-13	3.66E-12	*a*
		miR-145 Targets	−0.07	−0.05	−6.35	2.80E-09	1.19E-08	*e*
		miR-143 Targets	−0.06	−0.04	−5.95	2.04E-08	7.85E-08	*e*
		Gene CARMN	*Log2 fold change* 2.73	*Mean Expression* 1.43	8.82	4.72E-15	2.72E-13	
		Myc Signaling	−0.20	−0.24	−6.09	9.86E-09	3.91E-08	*a*

Top pathways characterizing subgroups of head and neck cancer cells from K2T scRNAseq analysis. The location of these subgroups in K2T derived model and distribution of pathway activity scores are shown in Fig. 1A–C.

a mSigDB Hallmarks of Cancer[34,35]

b Experimental

d Published[7]

c Published[10]

e TargetScan[36]

Table 2:

Cox Proportional Hazards Survival Testing Results of TCGA BRCA Bulk Gene Expression Projections onto Subgroup Gene Signatures

Subgroup	Clusters	Hazard Ratio	Z-score	P-value	FDR
M1	0	0.95	4.07	4.66E-05	0.001
B1	3, 0, 6, 1, 10	0.95	3.95	7.93E-05	0.001
A1	3, 0, 6, 13, 1, 8, 10, 12	−1.09	−3.22	1.30E-03	0.011
J2	8	−0.92	−2.94	3.30E-03	0.021
D1	3, 6	0.57	2.84	4.49E-03	0.023
K2	2	0.61	2.65	7.95E-03	0.034
L1	4	−0.89	−2.55	1.08E-02	0.036
E1	13	−0.54	−2.54	1.11E-02	0.036
B2	13, 8, 12	−0.47	−2.38	1.73E-02	0.050
F1	7	0.37	2.11	3.47E-02	0.090
M2	1	−0.60	−1.93	5.30E-02	0.125
D2	0, 1, 10	−0.46	−1.48	1.39E-01	0.302
F2	2, 11	0.22	1.35	1.76E-01	0.341
I1	0, 1	−0.43	−1.30	1.94E-01	0.341
A2	7, 9, 2, 5, 4, 11	0.18	1.29	1.99E-01	0.341
G2	5	−0.46	−1.24	2.14E-01	0.341
C1	7, 2, 11	−0.48	−1.22	2.23E-01	0.341
L2	9	−0.40	−1.18	2.40E-01	0.347
I2	10	−0.40	−1.12	2.61E-01	0.357
K1	11	0.17	0.92	3.56E-01	0.432
C2	9, 5, 4	0.13	0.92	3.58E-01	0.432
G1	9, 4	0.13	0.90	3.66E-01	0.432
H1	3	0.21	0.69	4.90E-01	0.554
H2	6	−0.10	−0.56	5.78E-01	0.626
J1	12	0.08	0.46	6.46E-01	0.672
E2	8, 12	0.08	0.23	8.21E-01	0.821

Statistical results from survival analyses, comparing signature projections derived from each subgroup on TCGA bulk gene expression data. The *Clusters* column indicates sets of cell clusters that belong to each subgroup label. For visualization, Kaplan-Meier curves for subgroups, F1, B2, E1, and J2 are shown in Fig. 1D.

Table 3:

Results of Pre-ranked GSEA Comparing Minimum Correlations of Gene Expression to mTORC1 and β-catenin/CBP and Annotated Gene Lists

	Name	Score	P-value	FDR	# Genes in Data Set
scRNAseq Data	β-catenin/CBP (E7386, Up-regulated)	0.24	1.00E-03	1.00E-03	954
	β-catenin/CBP (E7386, Down-regulated)	−0.06	1.00E-03	1.00E-03	1124
	β-catenin/CBP (ICG001, Up-regulated)	0.20	1.00E-03	1.00E-03	1200
	β-catenin/CBP (ICG001, Down-regulated)	−0.11	1.00E-03	1.00E-03	1324
	mTORC1	0.38	1.00E-03	1.00E-03	197
	p-EMT	0.31	1.00E-03	1.00E-03	100
	Raptor	0.49	1.00E-03	1.00E-03	106
TCGA HNSCC Data (All Tumor Samples)	β-catenin/CBP (E7386, Up-regulated)	0.33	1.00E-03	4.90E-02	930
	β-catenin/CBP (E7386, Down-regulated)	−0.07	1.00E-03	4.90E-02	1083
	β-catenin/CBP (ICG001, Up-regulated)	0.41	1.00E-03	4.90E-02	1172
	β-catenin/CBP (ICG001, Down-regulated)	−0.15	`1.00E-03	4.90E-02	1270
	mTORC1	0.39	1.00E-03	4.90E-02	196
	p-EMT	0.37	1.00E-03	4.90E-02	98
	Raptor	0.50	1.00E-03	4.90E-02	105
CCLE Data	β-catenin/CBP (E7386, Up-regulated)	0.31	1.00E-03	1.17E-03	919
	β-catenin/CBP (E7386, Down-regulated)	−0.14	1.00E-03	1.17E-03	1052
	β-catenin/CBP (ICG001, Up-regulated)	0.41	1.00E-03	1.17E-03	1149
	β-catenin/CBP (ICG001, Down-regulated)	−0.29	1.00E-03	1.17E-03	1224
	mTORC1	0.35	1.00E-03	1.17E-03	197
	p-EMT	−0.12	1.20E-01	1.20E-01	98
	Raptor	0.47	1.00E-03	1.17E-03	106